Supplementary Information

Thermodynamic inhibition of bromine-rich phase nucleation in wide-bandgap perovskites for operationally stable tandem solar cells

Xueying Yang,†[abg] Zhongliang Yan,†[abg] Shibo Wang,†[c] Pengfei Fu,†[ab] Chunyan Deng,[ab] Guang Yang,*[d] Yu Lou,[ab] Zhaojin Wang,[ab] Miao Zeng,[ab] You Chen,[ab] Zhicong Zhou,[ab] Xinyu Ye,[a] Xiaokang Sun,[e] Chengwei Shan,[f] Yuanmiao Sun,[a] Aung Ko Ko Kyaw,[f] Hanlin Hu,[e] Zhifang Shi,[b] Zaiwei Wang,[a] Xinbo Yang,*[c] Xiaohong Zhang,*[c] Gang Li,[d] Yang Bai*[abgj] and Hui-Ming Cheng*[ahi]

[a.] *Institute of Technology for Carbon Neutrality, Shenzhen Institutes of Advanced Technology (SIAT), Chinese Academy of Sciences, Shenzhen, China. E-mail: y.bai@siat.ac.cn, hm.cheng@siat.ac.cn*

[b.] *Faculty of Materials Science and Energy Engineering, Shenzhen University of Advanced Technology (SUAT), Shenzhen, China. E-mail: baiyang@suat-sz.edu.cn*

[c.] *College of Energy, Soochow Institute for Energy and Materials Innovations (SIEMIS); Institute of Functional Nano & Soft Materials (FUNSOM), Jiangsu Key Laboratory of Advanced Negative Carbon Technologies, Soochow University, Suzhou, China. E-mail: xbyang@suda.edu.cn, xiaohong_zhang@suda.edu.cn*

[d.] *Department of Electrical and Electronic Engineering, Photonic Research Institute (PRI), Research Institute of Smart Energy (RISE), Research Institute for Advanced Manufacturing (RIAM), The Hong Kong Polytechnic University, Hung Hom, Kowloon, Hong Kong, China. E-mail: guang.yg.yang@polyu.edu.hk*

[e.] *Hoffmann Institute of Advanced Materials, Shenzhen Polytechnic University, Shenzhen, China.*

[f.] *Department of Electronic & Electrical Engineering, Southern University of Science and Technology, Shenzhen, China.*

[g.] *University of Chinese Academy of Sciences, Beijing, China.*

[h.] *SKKU Global Research Center, Sungkyunkwan University, Suwon, Republic of Korea.*

[i.] *Shenyang National Laboratory for Materials Sciences, Institute of Metal Research, Chinese Academy of Sciences, Shenyang, China.*

[j.] *Perovseek Technology Co. Ltd, Yibin, China.*

† These authors contributed equally.

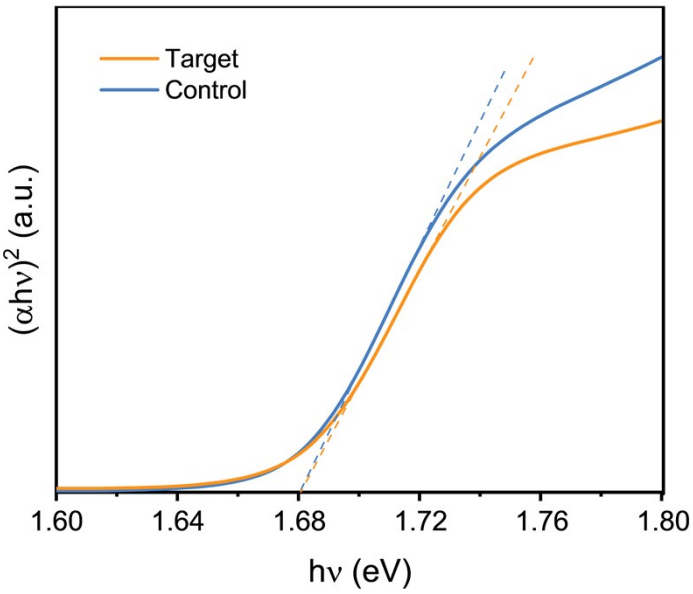

Fig. S1. Tauc plot showing comparable optical bandgaps for the control ($Cs_{0.05}MA_{0.15}FA_{0.8}Pb(I_{0.75}Br_{0.25})_3$) and target (with KSCN) perovskite thin films, with both formulations having an optical bandgap of 1.68 eV.

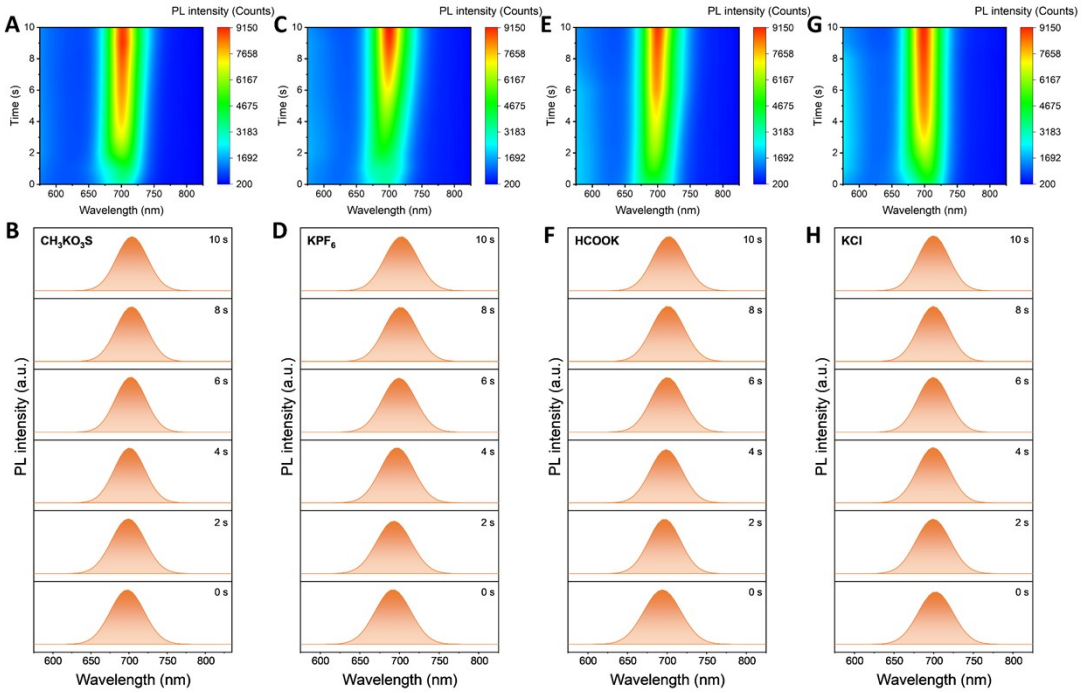

Fig. S2. In situ PL measurements during the perovskite spin-coating process: 2D images of In situ PL measurements during the spin-coating process of control perovskite with (A) CH_3KO_3S, (C) KPF_6, (E) HCOOK, (G) KCl. Extracted intensity-wavelength PL curves from the 2D image of control perovskite with (B) CH_3KO_3S, (D) KPF_6, (F) HCOOK, (H) KCl.

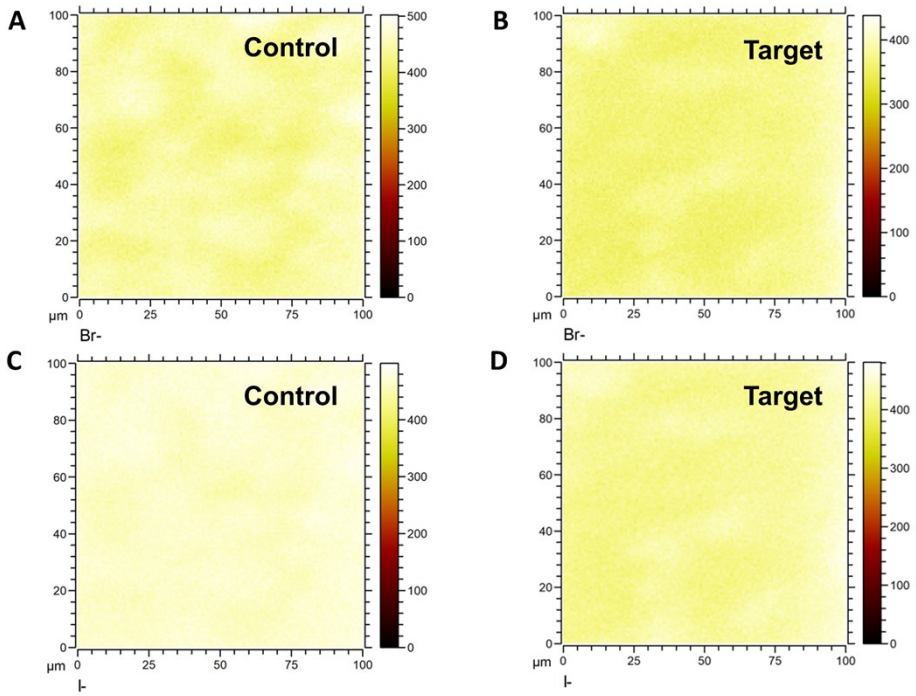

Fig. S3. Time-of-flight secondary ion mass spectrometry (TOF-SIMS) measurements: 2D distribution mapping of iodine in (A) control, and (B) target perovskite films, 2D distribution mapping of bromine in (C) control, and (D) target perovskite films.

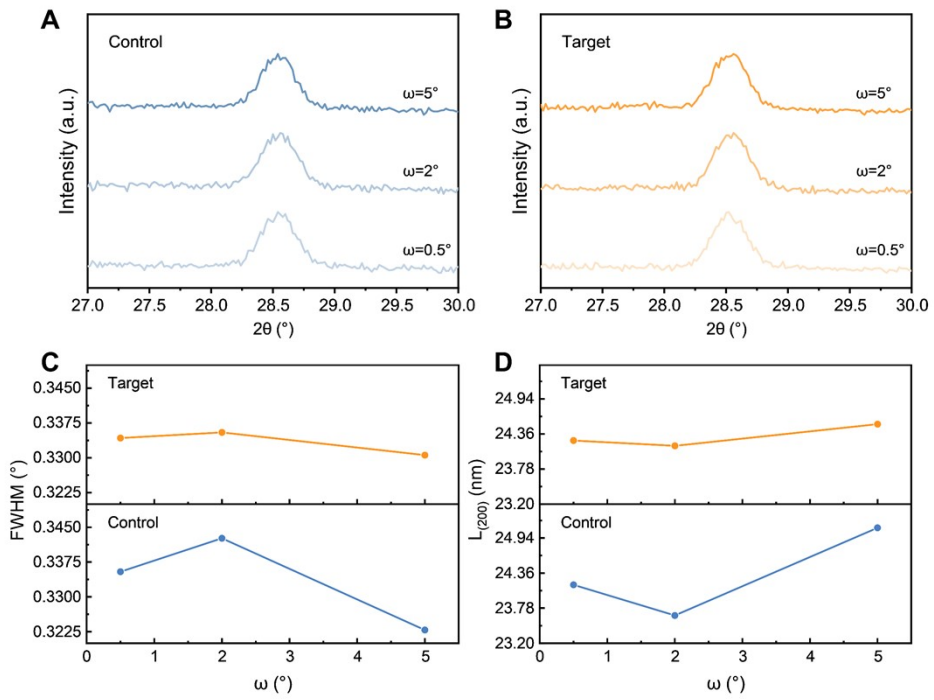

Fig. S4. GIXRD measurements: (A) GIXRD spectra around the perovskite (200) diffraction peaks collected at incident angles of 0.5°, 2°, and 5° for the Control film, (B) GIXRD spectra around the perovskite (200) diffraction peaks collected at incident angles of 0.5°, 2°, and 5° for the Target film, (C) The perovskite (200) diffraction peak full width at half-maximum (FWHM) for these two films are plotted as functions of incident angle in (A) and (B), (D) The perovskite (200) diffraction peak average size of crystalline domains for these two films are plotted as functions of incident angle in (C) and (D).

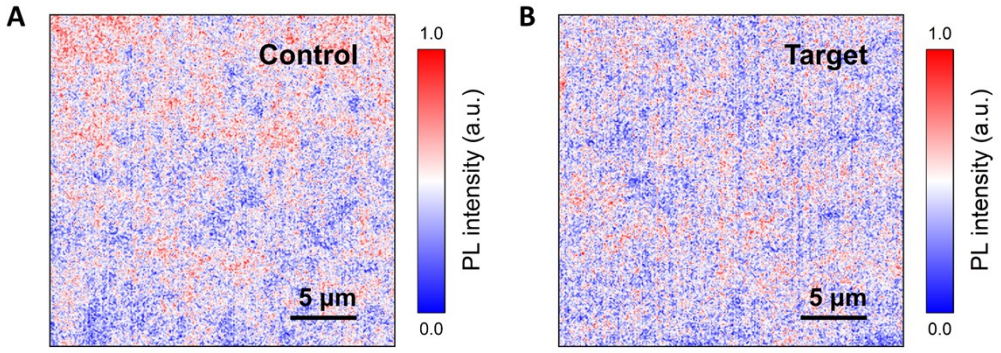

Fig. S5. PL mapping measurements: PL intensity distribution in (A) control, (B) target perovskite films. The scale bar is 5 μm.

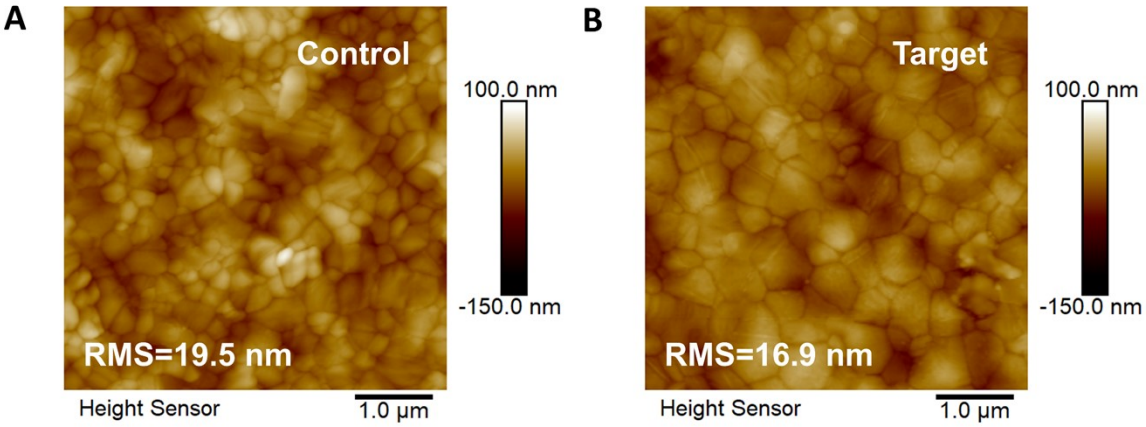

Fig. S6. Top-view atomic force microscope (AFM) images: (A) control perovskite film, (B) target perovskite film.

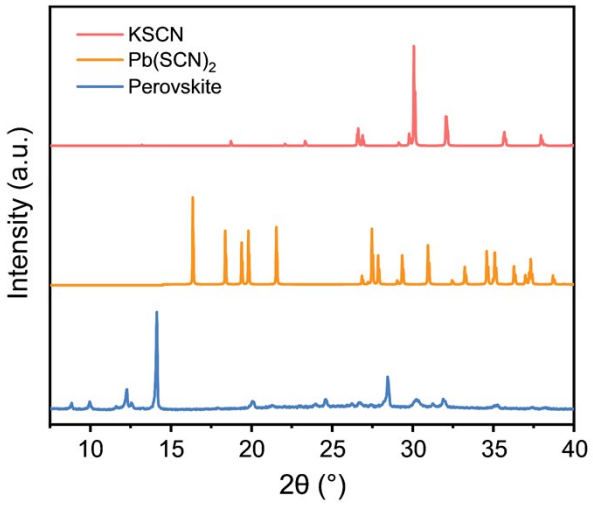

Fig. S7. XRD patterns of perovskite (with KSCN), pure $Pb(SCN)_2$ and pure KSCN.

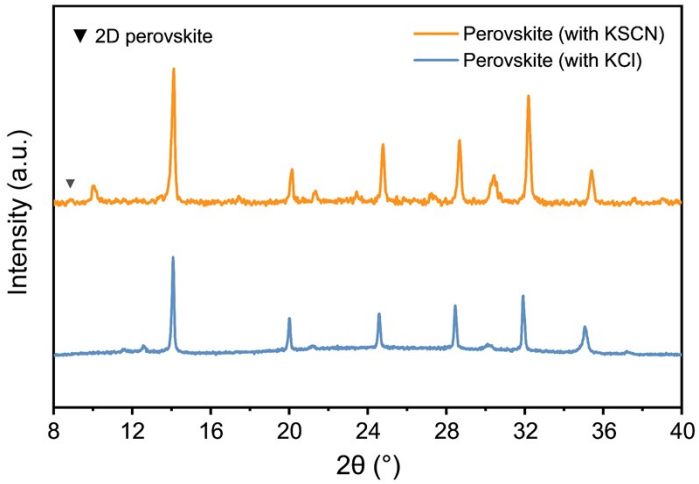

Fig. S8. XRD patterns of perovskite (with KSCN) and perovskite (with KCl).

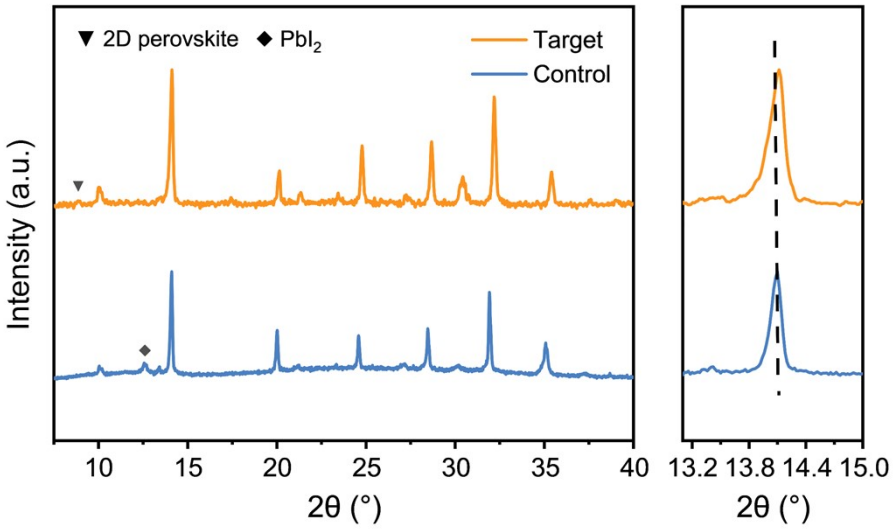

Fig. S9. XRD patterns of control and target perovskite film, and an enlargement of the range of 13.1-15.0°.

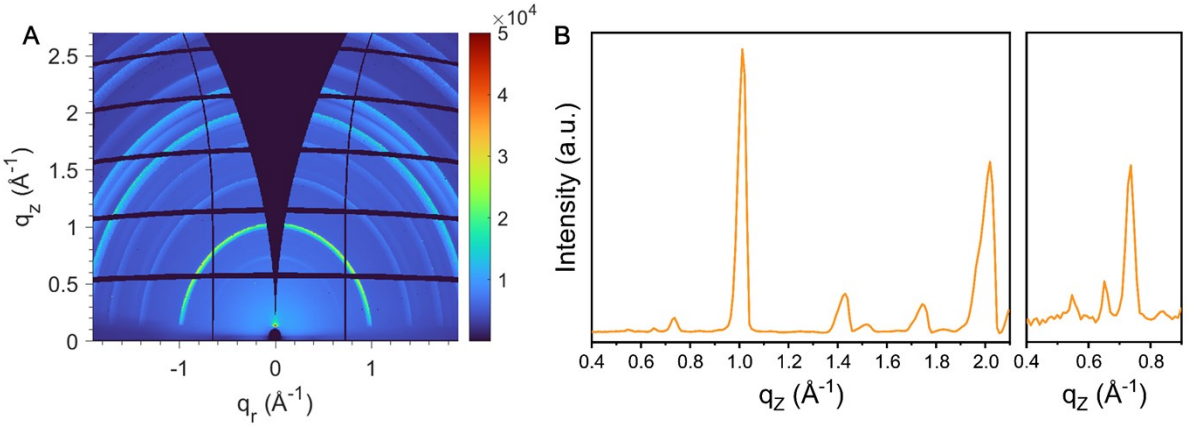

Fig. S10. GIWAXS patterns of target perovskite film. (A) Two-dimensional GIWAXS pattern of the target film. (B) Corresponding background-flattened intensity line profile extracted along q_z and an enlargement of the range of 0.4-0.9 $Å^{-1}$.

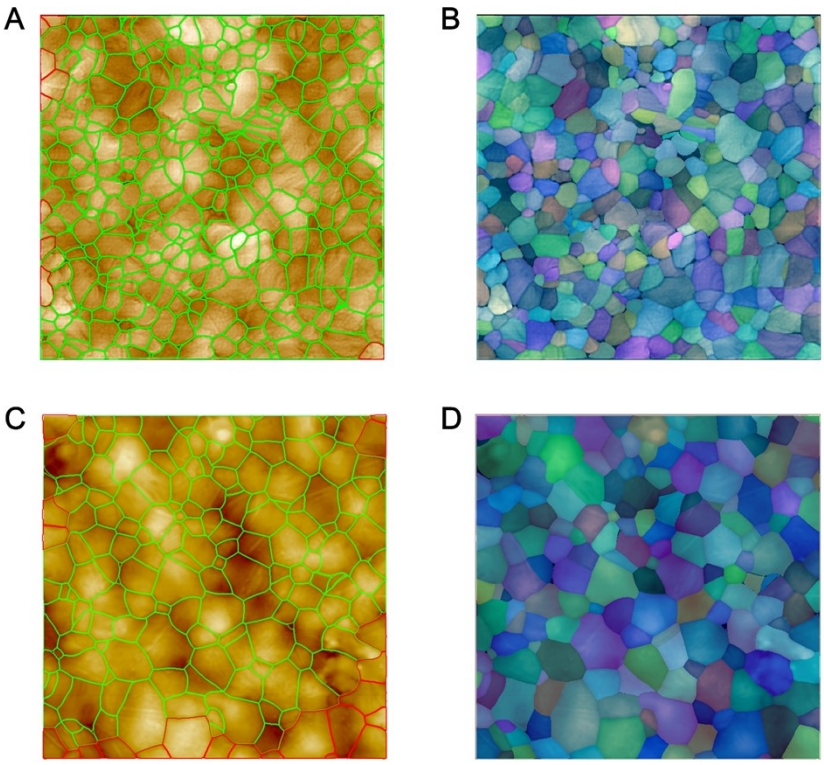

Fig. S11. Grain and grain boundary analysis of perovskite films. (A) A representative AFM image of the Control film with grain digitally outlined in green and red using an intelligent grain analysis platform. (B) The corresponding grain map, where each individual grain is assigned a distinct color to visualize size and distribution. Statistical analysis performed on multiple regions reveals a grain-boundary density of 15.20 μm^{-1}. (C) A representative AFM image of the Target film with grain digitally outlined in green and red using an intelligent grain analysis platform. (D) The corresponding grain map, where each individual grain is assigned a distinct color to visualize size and distribution. Statistical analysis performed on multiple regions reveals a grain-boundary density of 10.63 μm^{-1}.

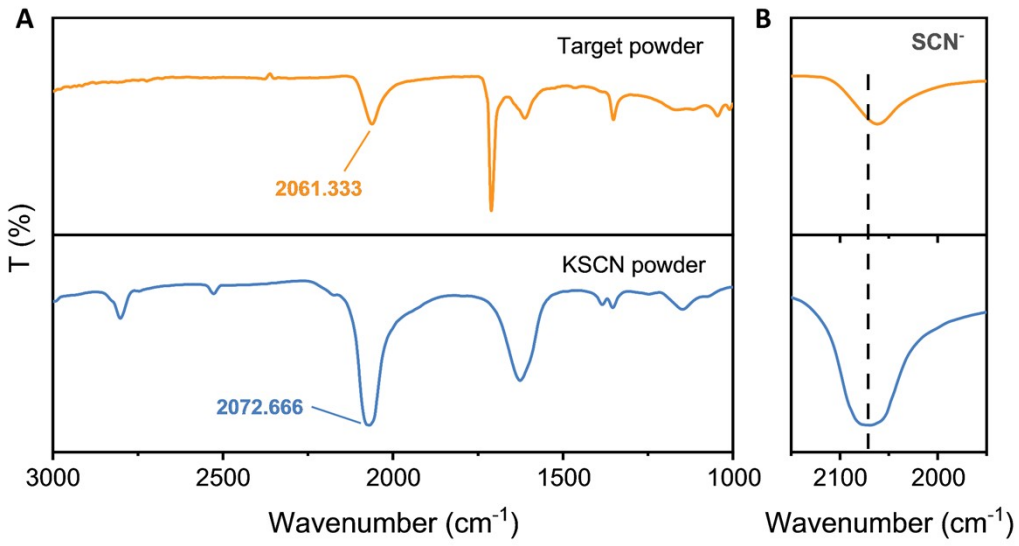

Fig. S12. Fourier transform infrared spectrometer (FTIR) measurements: (A) measurements on the target perovskite powder and pure KSCN powder at the range of 1000-3000 cm^{-1}, (B) enlarged stretching vibration frequency of SCN^- on the target perovskite powder and pure KSCN powder.

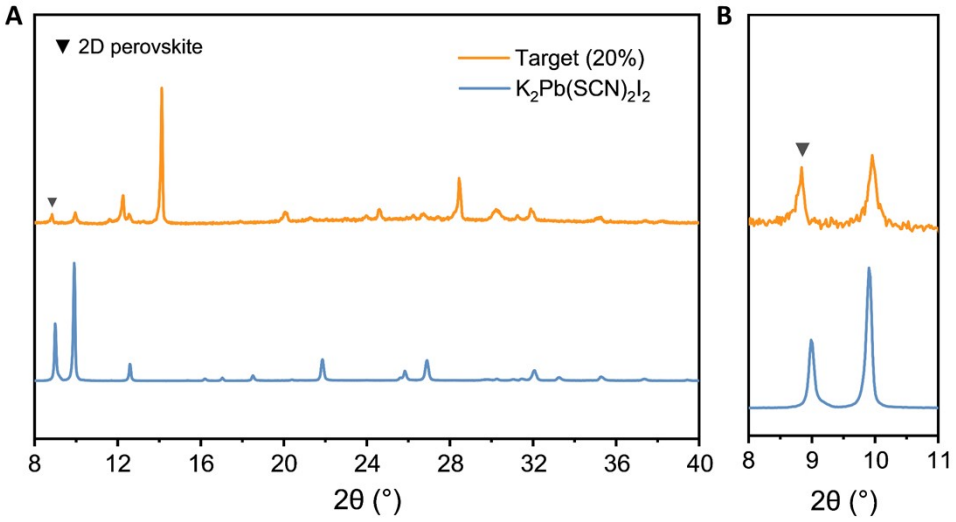

Fig. S13. XRD measurements: (A) measurement on target perovskite film with10x higher KSCN concentration and $K_2Pb(SCN)_2I_2$ 2D perovskite film, (B) magnification of the range 8-11°.

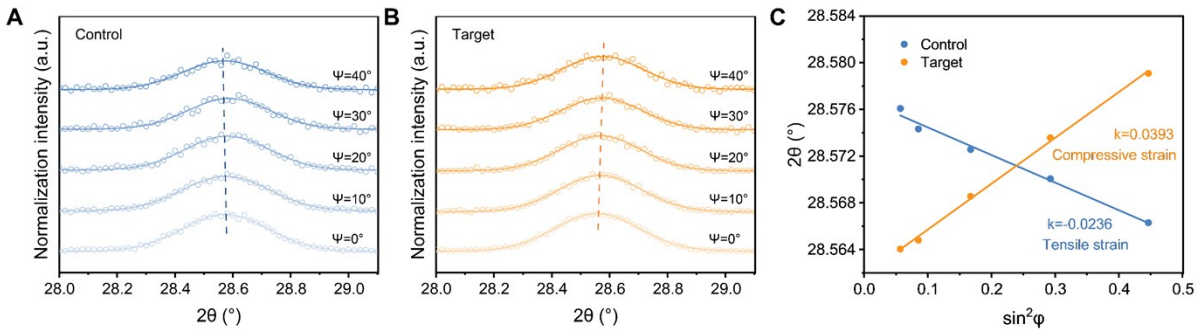

Fig. S14. GIXRD measurements: (A) GIXRD spectrum at different tilt angles with incident angle of 0.5º for the Control film, (B) GIXRD spectrum at different tilt angles with incident angle of 0.5º for the Target film, (C) Residual strain distribution for the films (measured (points) and Gauss fitted (line) diffraction strain data as a function of $\sin^2\varphi$).

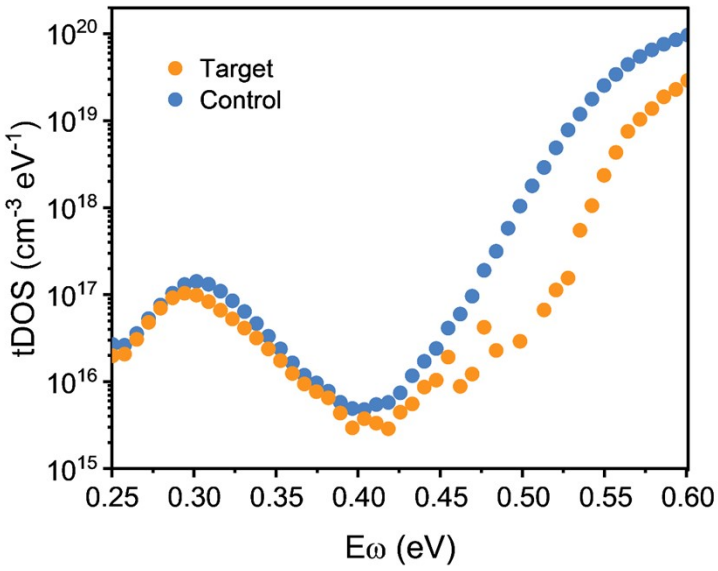

Fig. S15. tDOS spectra of control and target perovskite solar cells determined from temperature dependent capacitance-frequency measurement.

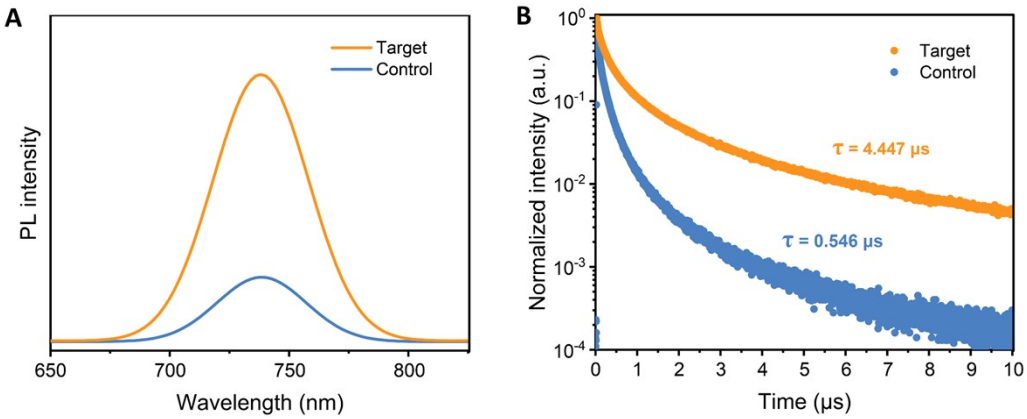

Fig. S16. Films measurements on the control and target perovskites: (A) photoluminescence (PL), (B) time-resolved photoluminescence (TRPL).

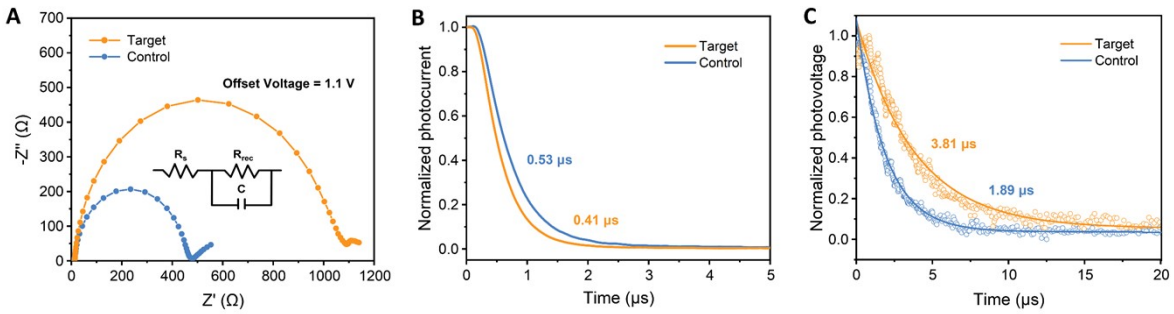

Fig. S17. Device measurements on the control and target perovskites: (A) impedance spectroscopy, (B) transient photocurrent, (C) transient photovoltage.

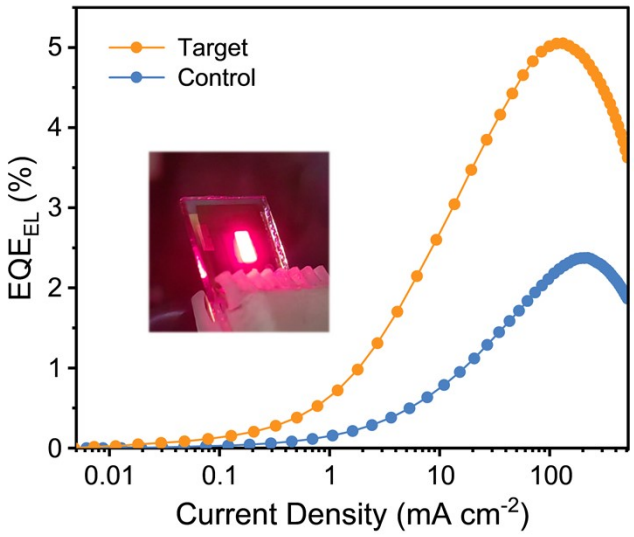

Fig. S18. EQE_{EL} of single-junction perovskite solar cells.

Test and Calibration Center of New Energy Device and Module,
Shanghai Institute of Microsystem and Information Technology,
Chinese Academy of Sciences (SIMIT)

Measurement Report

ReportNo. 24TR090908

Client Name	Xinbo Yang's Group, Soochow University
Client Address	No.688 Moye Road, Suzhou, Jiangsu, China
Sample	Perovskite/silicon tandem solar cell
Manufacturer	Xinbo Yang's Group, Soochow University
Measurement Date	9th September, 2024

Performed by:	Qiang Shi	Qiang Shi	**Date:** 09/09/2024
Reviewed by:	Wenjie Zhao	Wenjie Zhao	**Date:** 09/09/2024
Approved by:	Yucheng Liu	Yucheng Liu	**Date:** 09/09/2024

Address: No.235 Chengbei Road, Jiading, Shanghai **Post Code:**201800
E-mail: solarcell@mail.sim.ac.cn **Tel:** +86-021-69976905

Sample Information	
Sample Type	Perovskite/silicon tandem solar cell
Serial No.	70-8-2
Lab Internal No.	24090901-8#
Measurement Item	I-V characteristic
Measurement Environment	24.3±2.0°C, 43.7±5.0%R.H

Measurement of I-V characteristic	
Reference cell	PVM1121
Reference cell Type	mono-Si, WPVS, calibrated by NREL (Certificate No. ISO 2098)
Calibration Value/Date of Calibration for Reference cell	143.95mA/ Feb.2024
Measurement Conditions	Standard Test Condition(STC): SpectralDistribution: AM1.5, Irradiance: 1000±50W/m^2, Temperature: 25±2°C
Measurement Equipment/ Date of Calibration	AAA Steady State Solar Simulator (YSS-T155-2M) / Sep.2023 IV test system (ADCMT 6246) / June. 2024 Measuring Microscope (MF-B2017C) / July.2024 Spectral Response Measurement System(CEP-25ML-CAS) / May.2024
Measurement Method	I-V Measurement: Logarithmic sweep in both directions (Voc to Iscand Isc to Voc) during one flash based on IEC 60904-1:2020; Spectral Mismatch factor was calculated and I-V correction was performed according to IEC 60891.
Measurement Uncertainty	Area: 1.0%(k=2); Isc: 2.2%(k=2); Voc: 1.0%(k=2); Pmax: 2.8%(k=2); Eff: 2.9%(k=2)

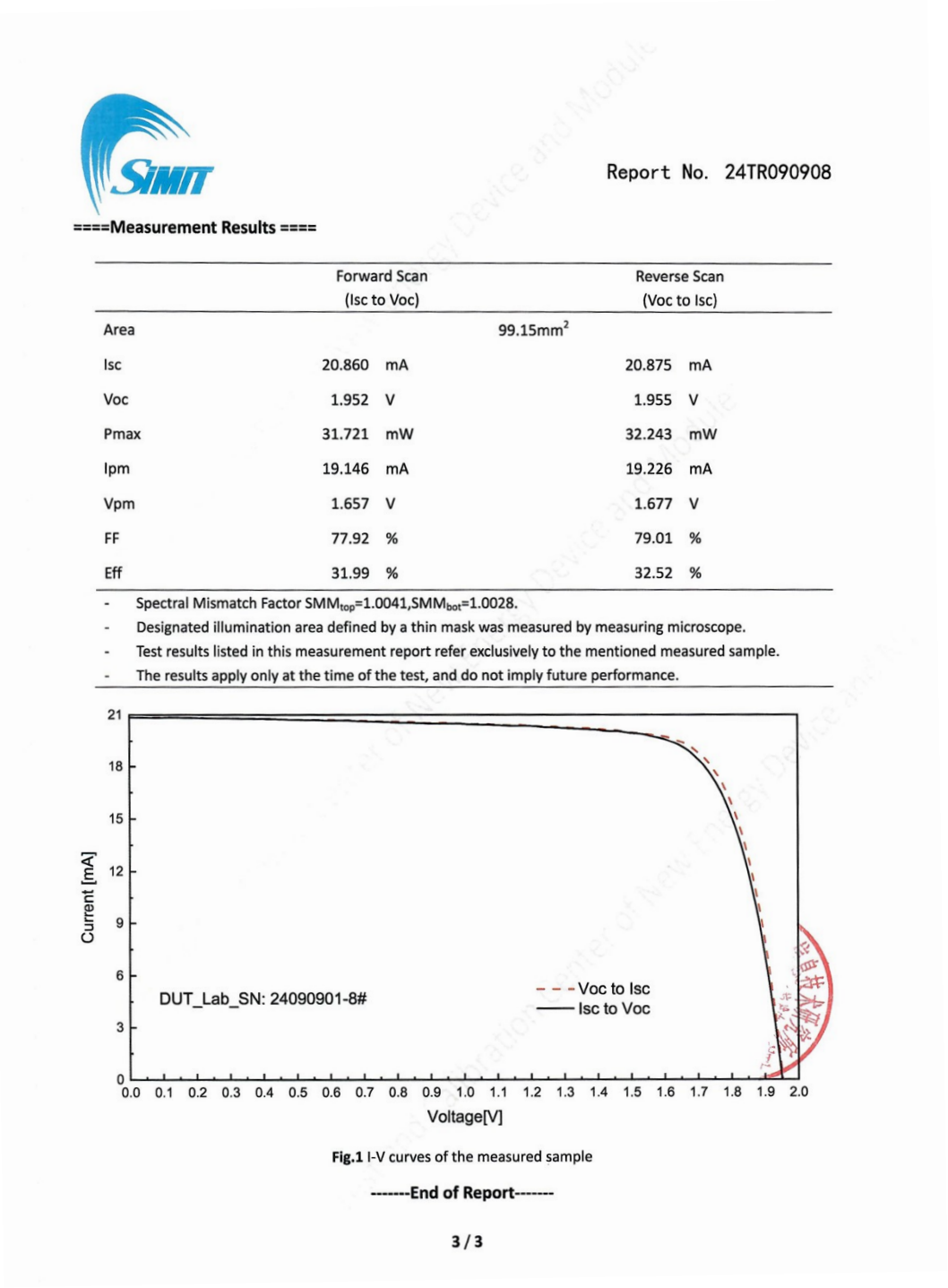

Report No. 24TR090908

====Measurement Results ====

	Forward Scan (Isc to Voc)	Reverse Scan (Voc to Isc)
Area	99.15mm^2	
Isc	20.860 mA	20.875 mA
Voc	1.952 V	1.955 V
Pmax	31.721 mW	32.243 mW
Ipm	19.146 mA	19.226 mA
Vpm	1.657 V	1.677 V
FF	77.92 %	79.01 %
Eff	31.99 %	32.52 %

- Spectral Mismatch Factor SMM_{top}=1.0041,SMM_{bot}=1.0028.
- Designated illumination area defined by a thin mask was measured by measuring microscope.
- Test results listed in this measurement report refer exclusively to the mentioned measured sample.
- The results apply only at the time of the test, and do not imply future performance.

Fig.1 I-V curves of the measured sample

-------End of Report-------

3 / 3

Fig. S19. Independent certification results of the perovskite-silicon tandem solar cell with a 0.9915 cm^2 aperture mask. The certifying authority is SIMIT (Test and Calibration Center of New Energy Device and Module, Shanghai Institute of Microsystem and Information Technology, Chinese Academy of Sciences).

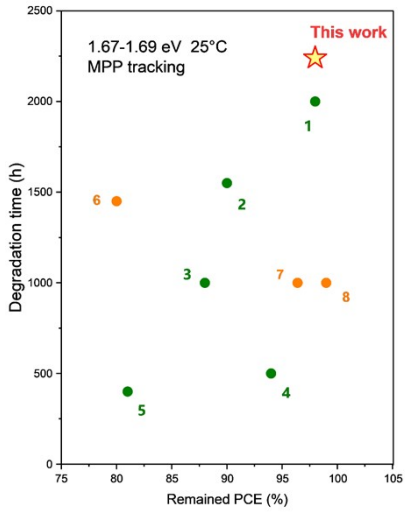

Fig. S20. Summary of the stability data of similar single-junction devices reported in recent years[1–8].

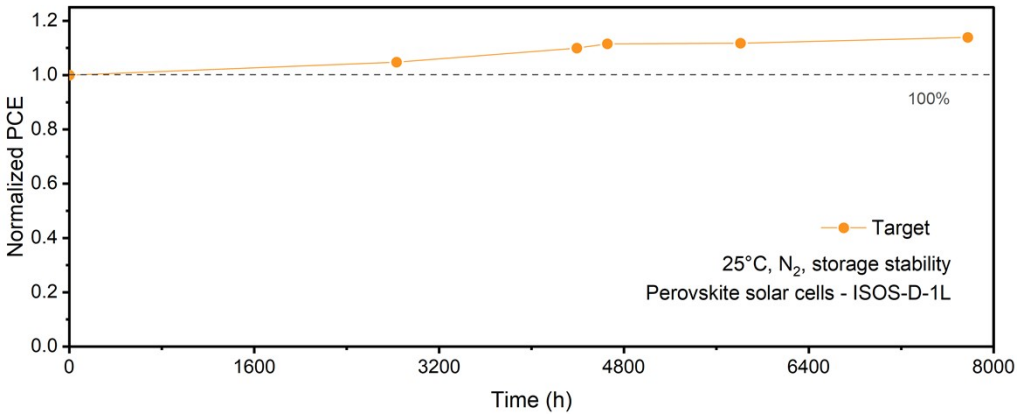

Fig. S21. Storage PCE tracking of the unencapsulated single-junction perovskite solar cells, 25°C, Compliant with Standard ISOS-D-1L.

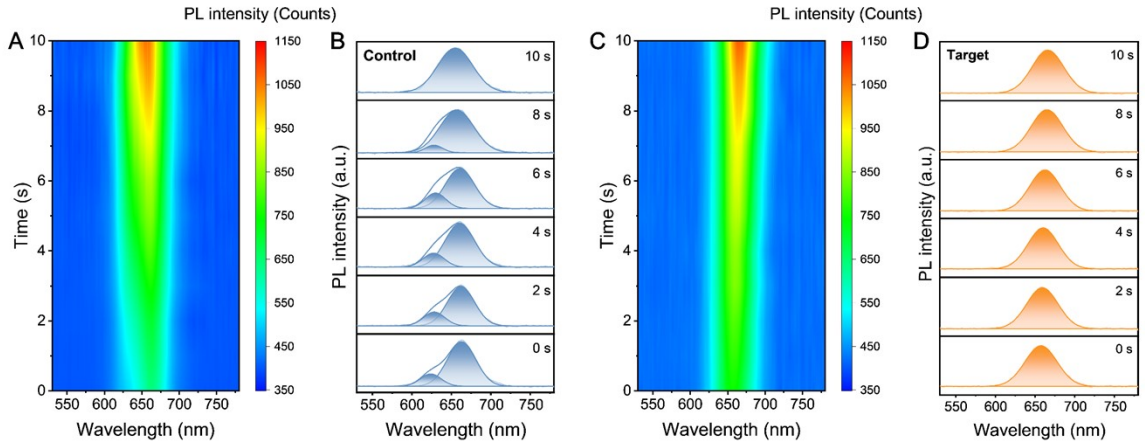

Fig. S22. Spin-coating of the 1.77 eV WBG perovskite film. (A) In-situ PL images during control perovskite spin-coating, with the moment of antisolvent drop marked as the 0 second, and the spin-coating process ending at the 10 second. (B) Extracted in-situ PL curves from (A). (C) In-situ PL images during target perovskite spin-coating, with the moment of antisolvent drop marked as the 0 second, and the spin-coating process ending at the 10 second. (D) Extracted in-situ PL curves from (C).

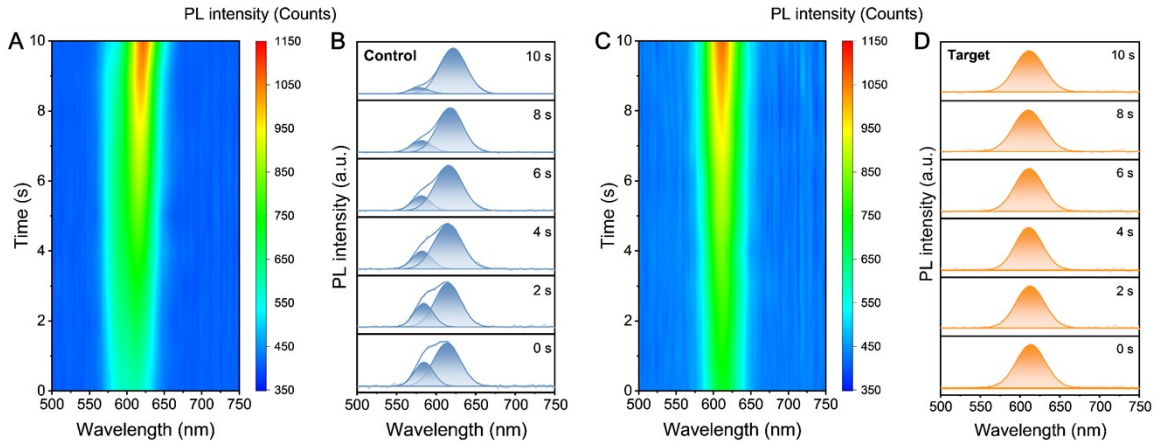

Fig. S23. Spin-coating of the 1.85 eV WBG perovskite film. (A) In-situ PL images during control perovskite spin-coating, with the moment of antisolvent drop marked as the 0 second, and the spin-coating process ending at the 10 second. (B) Extracted in-situ PL curves from (A). (C) In-situ PL images during target perovskite spin-coating, with the moment of antisolvent drop marked as the 0 second, and the spin-coating process ending at the 10 second. (D) Extracted in-situ PL curves from (C).

CPVT
国家光伏质检中心

检验检测报告

TEST REPORT

No:2025DMCS20129

产品名称 SAMPLE	全钙钛矿叠层太阳能电池 All-perovskite Tandem Solar Cells
规格型号 MODEL/TYPE	15 mm *15 mm
委托单位 APPLICANT	中国科学院深圳先进技术研究院 / 深圳理工大学 Shenzhen Institute of Advanced Technology, Chinese Academy of Sciences / Shenzhen University of Advanced Technology

无锡市检验检测认证研究院

Wuxi Institute of Inspection, Testing and Certification

国家太阳能光伏产品质量检验检测中心

National Center of Inspection on Solar Photovoltaic Products Quality

检 验 检 测 结 果
Test Results

序号 Clause	检验项目 Test item(s)	单位 Unit	技术要求 Technical requirements	结果 Results	单项评价 Verdict Pass/Fail
1	电流-电压特性的测量(正扫) Current-voltage characteristic measurement (Forward scan)	—	在标准试验条件下（样品温度：25℃±2℃，辐照度：1000W/ m²，标准太阳光谱辐照分布符合 IEC 60904-3 规定），测量样品随负荷变化的电流-电压特性。 At STC (module temperature: 25℃±2℃, irradiance: 1000W/m², standard solar spectral irradiance distribution corresponds to IEC60904-3), measure the current-voltage characteristics of the cell with the variation of load.	—	—
1.1	开路电压 Voc Open-circuit voltage, Voc	V	—	2.149	—
1.2	短路电流 Isc Short-circuit current, Isc	mA	—	0.8046	—
1.3	最大功率 Pmax Maximum-power, Pmax	mW	—	1.401	—
1.4	最大功率点电压 Vmp Maximum-power voltage, Vmp	V	—	1.860	—
1.5	最大功率点电流 Imp Maximum-power current, Imp	mA	—	0.7535	—
1.6	填充因子 FF，% Fill factor FF, %	—	—	81.03	—
1.7	转换效率 η，% Conversion efficiency η, %	—	$\eta = \frac{P_{max}}{1000W/m^2 \times S} \times 100\%$ S 为掩膜板面积/Area S is determined by mask	27.69	—

备注：正扫扫描方向为-0.1V~2.24V，步进 0.02V，延迟时间：0.1 s；短路电流密度$J_{sc} = \frac{I_{sc}}{S}$ =15.90 mA/cm²。
计算短路电流密度及转换效率所用面积为掩膜板面积，S=5.059 mm²。

Remark: Forward sweep direction: -0.1V~2.24V, step: 0.02V, delay time :0.1s. $J_{sc} = \frac{I_{sc}}{S}$ =15.90 mA/cm²
The area used to calculate J_{sc} and Conversion efficiency is determined by mask, S=5.059 mm².

检 验 检 测 结 果
Test Results

序号 Clause	检验项目 Test item(s)	单位 Unit	技术要求 Technical requirements	结果 Results	单项评价 Verdict Pass/Fail
2	电流-电压特性的测量 (反扫) Current-voltage characteristic measurement (Reverse Scan)	—	在标准试验条件下（样品温度：25℃±2℃，辐照度：1000W/ m²，标准太阳光谱辐照分布符合 IEC 60904-3 规定），测量样品随负荷变化的电流-电压特性。 At STC (module temperature: 25℃±2℃, irradiance: 1000W/m², standard solar spectral irradiance distribution corresponds to IEC60904-3), measure the current-voltage characteristics of the cell with the variation of load.	—	—
2.1	开路电压 Voc Open-circuit voltage, Voc	V	—	2.154	—
2.2	短路电流 Isc Short-circuit current, Isc	mA	—	0.8000	—
2.3	最大功率 Pmax Maximum-power, Pmax	mW	—	1.425	—
2.4	最大功率点电压 Vmp Maximum-power voltage, Vmp	V	—	1.880	—
2.5	最大功率点电流 Imp Maximum-power current, Imp	mA	—	0.7578	—
2.6	填充因子 FF，% Fill factor FF, %	—	—	82.69	—
2.7	转换效率 η，% Conversion efficiency η, %	—	$\eta = \frac{P_{max}}{1000W/m^2 \times S} \times 100\%$ S 为掩膜板面积/Area S is determined by mask	28.17	—

备注：反扫扫描方向为 2.24V~-0.1V，步进-0.02V，延迟时间：0.1 s；短路电流密度$J_{sc} = \frac{I_{sc}}{S}$ =15.81 mA/cm²。计算短路电流密度及转换效率所用面积为掩膜板面积，S=5.059 mm²。

Remark: Reverse sweep direction: 2.24V~-0.1 V, step: -0.02V, delay time :0.1s. $J_{sc} = \frac{I_{sc}}{S}$ =15.81 mA/cm²
The area used to calculate J_{sc} and Conversion efficiency is determined by mask, S=5.059 mm².

检 验 检 测 结 果
Test Results

标准试验条件下电流-电压特性曲线
Current-voltage characteristic Curve at STC

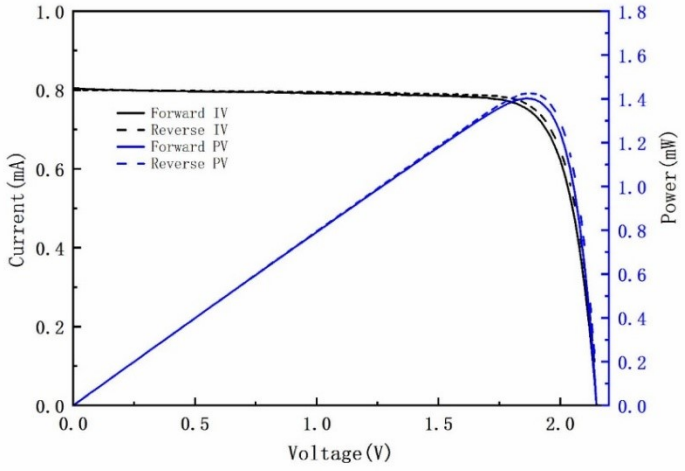

备注：—
Remark: —

No:2025DMCS20129 共 8 页 第 5 页 page 5 of 8

检 验 检 测 结 果
Test Results

序号 Clause	检验项目 Test item(s)	单位 Unit	技术要求 Technical requirements	结果 Results	单项评价 Verdict Pass/Fail
3	最大功率点测量 (最大功率点跟踪法) Maximum-power measurement (MPPT measurement method)	—	在标准试验条件下（样品温度：25℃±2℃，辐照度：1000W/ m², 标准太阳光谱辐照分布符合 IEC 60904-3 规定），对样品最大功率点持续扫描 5 min，取样品最后 5min 测量数据的平均值。 At STC (module temperature: 25℃ ±2℃, irradiance: 1000W/m², standard solar spectral irradiance distribution corresponds to IEC60904-3), continuously scan the maximum power of sample for 5 min, take the average Pmax of last 5 min.	—	—
3.1	最大功率 Pmax Maximum-power, Pmax	mW	—	1.376	—
3.2	转换效率 η，% Conversion efficiency η, %	—	$\eta = \frac{P_{max}}{1000W/m^2 \times S} \times 100\%$ S 为掩膜板面积/Area S is determined by mask	27.20	—

稳态扫描曲线
Steady-state scanning

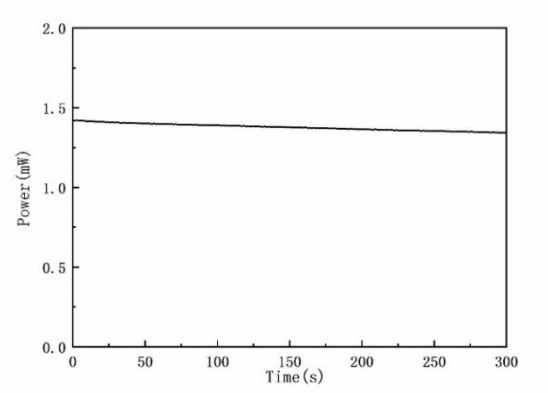

备注/ Remark： S=5.059 mm²

Fig. S24. Independent certification results of the all-perovskite tandem solar cell with a 5.059 mm² aperture mask. The certifying authority is CPTV (National Center of Inspection on Solar Photovoltaic Products Quality).

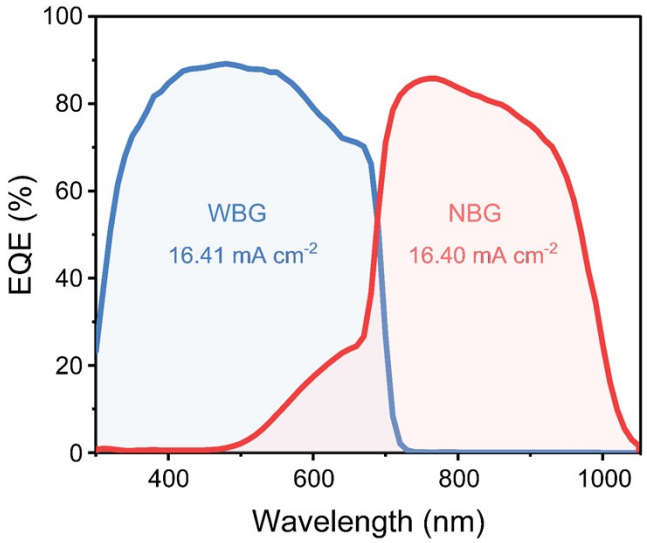

Fig. S25. EQE of all-perovskite tandem solar cell.

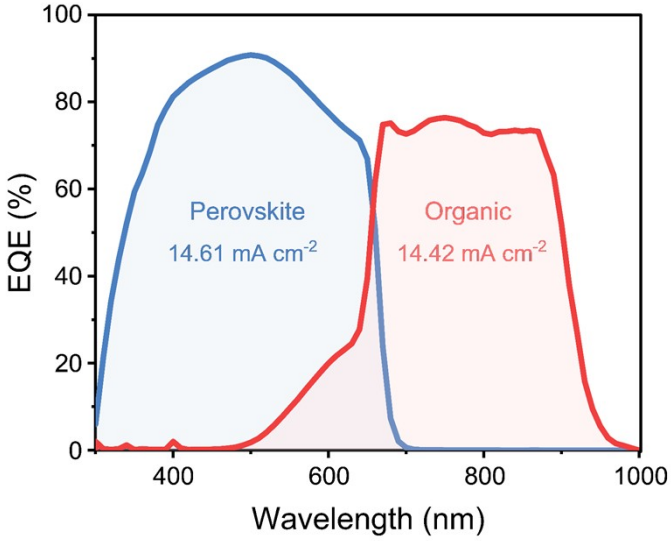

Fig. S26. EQE of perovskite-organic tandem solar cell.

Table S1. Formation energy calculations for $CsPbBr_3$, $CsPbI_3$, $KPbBr_3$ and $KPbI_3$ perovskite.

	$CsPbBr_3$	$CsPbI_3$	$KPbBr_3$	$KPbI_3$
Formation Energy (meV/f.u.)	-164.23	56.39	303.39	481.62

Table S2. Specific parameters of J-V measurements of 1.68 eV control, target and perovskite-silicon tandem devices.

Device	V_{OC} (V)	J_{SC} (mA cm^{-2})	FF (%)	PCE (%)
Control-Forward	1.258	21.21	81.70	21.84
Control-Reverse	1.250	20.95	80.56	21.13
Target-Forward	1.289	21.79	83.53	23.50
Target-Reverse	1.278	21.74	84.00	23.36
Tandem	1.985	20.57	81.04	33.08

Table S3. Detailed parameters for each voltage loss component of the V_{OC}-loss measurement.

Device	Bandgap (eV)	$V_{OC, SQ}$ (V)	ΔV_1 (V)	$V_{OC, rad}$ (V)	ΔV_2 (V)	$V_{OC, cal}$ (V)	ΔV_3 (V)	V_{OC} loss (V)
Control	1.682	1.402	0.280	1.381	0.022	1.253	0.128	0.430
Target	1.679	1.400	0.279	1.380	0.020	1.294	0.086	0.385

Table S4. Specific parameters of J-V measurements of target 1.77 eV single-junction and all-perovskite tandem devices.

Device	V_{OC} (V)	J_{SC} (mA cm^{-2})	FF (%)	PCE (%)
Single-junction	1.340	18.33	82.93	20.37
Tandem	2.124	16.50	80.41	28.18

Table S5. Specific parameters of J-V measurements of target 1.88 eV single-junction and perovskite-organic tandem devices.

Device	V_{OC} (V)	J_{SC} (mA cm^{-2})	FF (%)	PCE (%)
Single-junction	1.385	16.34	80.00	18.11
Tandem	2.144	15.69	77.00	25.66

Note S1. Outdoor Performance Retention Calculation Details

1. Power Conversion Efficiency (PCE) Formula:

The PCE is defined as the ratio of the electrical output power to the incident input power from solar irradiation:

$$PCE = \frac{P_{out}}{P_{in}} = \frac{P_{out}}{E \times A}$$

where: $P_{out}\,(W)$ is the output power, $P_{in}\,(W)$ is the input power, calculated as the product of solar irradiance $E\,(W/m^2)$ and the device active area $A\,(m^2)$.

2. Performance Retention Calculation:

Performance retention is the ratio of the final PCE to the initial PCE, expressed as a percentage:

$$Performance\ retention = \frac{PCE_{final}}{PCE_{initial}} \times 100\% = \frac{P_{out,final}/(E_{final} \times A)}{P_{out,\ initial}/(E_{initial} \times A)} \times 100\%$$

Since A is constant, this simplifies to:

$$Performance\ retention = \frac{P_{out,final}}{E_{final}} \times \frac{E_{initial}}{P_{out,\ initial}} \times 100\%$$

3. Calculation for 540-hour Outdoor Test (ISOS-O-2):

Input Data:

$P_{out,inatial} = 17.20\ mW = 0.01720\ W$

$E_{initial} = 757.06\ W/m^2$

$P_{out,final} = 19.90\ mW = 0.01823\ W$

$E_{final} = 758.84\ W/m^2$

Step-by-Step Calculation:

$$Performance\ retention = \frac{0.01823}{758.84} \times \frac{757.06}{0.01720} \times 100\% = 105.74\%$$

References

1 L. Qiao, T. Ye, T. Wang, W. Kong, R. Sun, L. Zhang, P. Wang, Z. Ge, Y. Peng, X. Zhang, M. Xu, X. Yan, J. Yang, X. Zhang, F. Zeng, L. Han and X. Yang, *Advanced Energy Materials*, 2024, **14**, 2302983.

2 X. Niu, N. Li, Z. Cui, L. Li, F. Pei, Y. Lan, Q. Song, Y. Du, J. Dou, Z. Bao, L. Wang, H. Liu, K. Li, X. Zhang, Z. Huang, L. Wang, W. Zhou, G. Yuan, Y. Chen, H. Zhou, C. Zhu, G. Liu, Y. Bai and Q. Chen, *Advanced Materials*, 2023, **35**, 2305822.

3 T. Nie, Z. Fang, T. Yang, K. Zhao, J. Ding and S. (Frank) Liu, *Angewandte Chemie*, 2024, **136**, e202400205.

4 Y. Song, Z. Liu, X. Cai, H. Ge, X. Liu, X. Wang, A. Li, T. Miyasaka, N. Shibayama and X.-F. Wang, *Advanced Energy Materials*, 2025, 2500650.

5 X. Zhou, X. Li, B. Shi, P. Wang, X. Du, Y. Zhao and X. Zhang, *ACS Nano*, 2025, **19**, 11187–11196.

6 A. S. Subbiah, S. Mannar, V. Hnapovskyi, A. R. Pininti, B. Vishal, L. V. Torres Merino, O. Matiash, O. Karalis, H. Hempel, A. Prasetio, B. Yildirim, P. Dally, D. Rosas Villalva, M. Babics, L. Xu, A. Razzaq, R. Azmi, F. Xu, H. L. Bristow, E. Ugur, A. Ur Rehman, H. Pasanen, E. Aydin, T. Allen, D. Baran, T. Unold, F. Laquai and S. De Wolf, *Joule*, 2025, **9**, 101767.

7 F. Scheler, S. Mariotti, D. Mantione, S. Shah, D. Menzel, H. Köbler, M. Simmonds, T. W. Gries, J. Kurpiers, V. Škorjanc, J. Li, A. Al-Ashouri, P. Wagner, S. P. Harvey, F. Yang, M. Rusu, T. Unold, B. Stannowski, K. Zhu, F. Lang, D. Neher, E. Unger, A. Abate, D. Mecerreyes, M. Stolterfoht, E. Köhnen, L. Korte, M. Topič and S. Albrecht, *Advanced Energy Materials*, 2025, **15**, 2404726.

8 S. G. Ji, I. J. Park, H. Chang, J. H. Park, G. P. Hong, B. K. Choi, J. H. Jang, Y. J. Choi, H. W. Lim, Y. J. Ahn, S. J. Park, K. T. Nam, T. Hyeon, J. Park, D. H. Kim and J. Y. Kim, *Joule*, 2022, **6**, 2390–2405.